

Asteroid flux towards circumprimary habitable zones in binary star systems: II. Dynamics

D. Bancelin^{1,2}, E. Pilat-Lohinger¹, and Á. Bazsó¹

¹ Institute of Astrophysics (ifA), University of Vienna, Türkenschanzstr. 17, A-1180 Vienna, Austria (e-mail: david.bancelin@univie.ac.at)

² IMCCE, Paris Observatory, UPMC, CNRS, UMR8028, 77, Av. Denfert-Rochereau F-75014 Paris, France

Received —, 2011; accepted —

ABSTRACT

Context. Secular and mean motion resonances (hereafter MMR) are effective perturbations to shape planetary systems. In binary star systems, they play a key role during the early and late phases of planetary formation as well as for the dynamical stability of a planetary system.

Aims. In this study, we aim to correlate the presence of orbital resonances with the rate of icy asteroids crossing the habitable zone (hereafter HZ), from a circumprimary disk of planetesimals in various binary star systems.

Methods. We modelled a belt of small bodies in the inner and outer regions, interior and exterior to the orbit of a gas giant planet respectively. The planetesimals are equally placed around a primary G-type star and move under the gravitational influence of the two stars and the gas giant. We numerically integrated the system for 50 Myr considering various parameters for the secondary star. Its stellar type varies from a M- to F-type; its semimajor axis is either 50 au or 100 au and its eccentricity is either 0.1 or 0.3. For comparison, we also varied the gas giant's orbital and physical parameters.

Results. Our simulations highlight that a disk of planetesimals will suffer from perturbations due to a perturbed gas giant, mean motion and secular resonances. We show that a secular resonance – with location and width varying according to the secondary star's characteristics – can exist in the icy asteroid belt region and overlap with MMRs which will have an impact on the dynamical lifetime of the disk. In addition, we point out that in any case, the 2:1 MMR, the 5:3 MMR and the secular resonance are powerful perturbations for the flux of icy asteroids towards the HZ and the transport of water therein.

Key words. Celestial mechanics – Methods: numerical – Minor planets, asteroids: general – binaries: general

1. Introduction

Orbital resonances (mean motion and secular resonances) play a key role in the architecture of a planetary system. It is well known that they had a strong influence on the dynamics in the early stage [Walsh et al., 2011] and late stage [Tsiganis et al., 2005, Gomes et al., 2005] of the planetary formation in our solar system. More generally, the late phase of planetary formation around single stars is mainly dominated by MMRs as a gas giant could have formed within 10 Myr [Briceño et al., 2001].

The role of a secular perturbation is mainly critical during the early phases of planetary formation in binary systems [Thebault and Haghighipour, 2014, and references therein] as it influences the collisional velocities between planetesimals. However, if planets manage to form despite these strong perturbations, their dynamical outcome will anyway be governed by MMR and secular resonances, which will determine the well-known stability criteria in binary star systems [Rabl and Dvorak, 1988, Holman and Wiegert, 1999, Pilat-Lohinger and Dvorak, 2002, Mudryk and Wu, 2006]. Location of orbital resonances have to be known in order to predict the fate of bodies evolving close or inside. The location of the secular resonance can be determined analytically by the Laplace-Lagrange perturbation theory [e.g. Murray and Dermott, 1999] provided that the planets have low eccentricities and inclinations and negligible masses compared to the central star. In this context,

Pilat-Lohinger et al. [2008] analysed the effect of different Jupiter-Saturn configurations by varying the mutual distance and the mass-ratio of the two planets. They showed that for some configurations, the HZ of the Sun would be affected by a secular resonance whose frequency $g = g_{\text{Jupiter}}$, with g_{Jupiter} the proper secular frequency of Jupiter (as defined in the Laplace-Lagrange theory). Moreover, it was shown that the analytical result was in good agreement with that of the numerical study. An application of this secular perturbation theory to circumstellar planetary motion in binary star systems causes problems in the accuracy due to the massive secondary star which often moves in an eccentric orbit around the center of mass. In Pilat-Lohinger et al. [2016], it was shown that the secular resonance which occurs in tight binary star systems hosting a giant planet [see e.g. Pilat-Lohinger, 2005] can be located by a semi-analytical method. This method uses the Laplace-Lagrange perturbation theory to determine the proper frequencies of test planets in such binary star-planet configurations while the frequency of the giant planet is calculated from a numerical time series via fast Fourier transformation. The location of the secular resonance is given by the intersection of the two resulting curves. An application of this method to all known binary star systems hosting a giant planet in circumstellar motion is presented in the paper by Bazsó et al. [2016].

Icy bodies trapped into orbital resonances could be potential water sources for planets in the HZ. These water rich

objects can be embryos [Haghighipour and Raymond, 2007] and small bodies (asteroids) as shown in Morbidelli et al. [2000] and O’Brien et al. [2014] for our Earth and more recently in Bancelin et al. [2015] (hereafter Paper I) in binary star systems. In this latter study, the author gave a statistical estimate of the contribution of asteroids in bearing water material to the HZ. Previous studies in binary star systems [e.g. Haghighipour and Raymond, 2007] focused mainly on the water transport via embryos.

This study is a continuation of the investigation from Paper I and elucidates dynamical features of this work. In Paper I, we showed a statistical overview about the flux of asteroids towards the circumprimary HZ of a binary star systems. Considering different binary configurations, we determined the timescale for an asteroid to reach the HZ (which is in the range between a few centuries and some ten thousands years) and provided estimates for the probability for an asteroid to cross the HZ (1 – 50%) and the quantity of water brought to the HZ (ratio of 1 – 15). In the present study, in order to explain the differences in the statistical results, we aim to emphasize and characterize the dynamical effects of orbital resonances on a disk of planetesimals, in various binary star systems hosting a gas giant planet, as well as to what extent such resonances are likely to enable icy asteroids to bring water material into the HZ in comparison to single star systems. In section 2, we define our initial modelling for the binary star systems, the gas giant and the disk of planetesimals. Then in section 3, we discuss their dynamical outcome. We also analyse the dynamical behaviour of particles initially orbiting near or inside MMRs in order to highlight the discrepancies on the dynamical lifetime according to the binary star system investigated. In section 4, we combine our results to analyse the consequences of such dynamics on the flux of icy asteroids towards the HZ and the water transport therein. We then analyse how the previous results are influenced when changing the orbital and physical parameters of the gas giant (section 5.1) or when one or two giant planets orbit around one G2V star (section 5.2). Finally, we provide a comparison of the water transport efficiency between binary and single star systems in section 6 and conclude our work in section 7.

2. Dynamical model

We focused our work on a primary G-type star but the secondary is either an F-, G-, K- or M-type star with mass M_b equal to $1.3M_\odot$, $1.0M_\odot$, $0.7M_\odot$ and $0.4M_\odot$ respectively. The orbital separations are $a_b = 50$ au and 100 au. The secondary’s eccentricity is $e_b = 0.1$ and 0.3; its inclination is set to 0° . Our systems host also a gas giant planet initially at $a_{GG} = 5.2$ au moving on a circular orbit, in the same plane as the secondary, and with a mass $M_{GG} = 1M_J$, M_J being the mass of Jupiter.

We modelled a disk of planetesimals inside and beyond the orbit of the gas giant. In order to avoid strong initial interaction with the gas giant, we assumed that it has gravitationally cleared a path in the disk around its orbit. We defined the width of this path as $\pm 3R_{H,GG}$, where $R_{H,GG}$ is the giant planet’s Hill radius. Contrary to Paper I in which the small bodies were randomly placed beyond the snow-line, we considered a different initial set up of the planetesimal disk in order to allow easy comparisons of the dynamics in the various systems. We defined three different regions in our planetesimal disk:

Table 1. Stability limits a_c for the considered binary configurations. For the values of a_c , we applied the results by Pilat-Lohinger and Dvorak [2002]

Secondary star	e_b	a_c [au]	a_c [au]
		($a_b = 50$ au)	($a_b = 100$ au)
F	0.1	11.9	23.8
	0.3	7.9	11.8
G	0.1	12.5	25.0
	0.3	8.0	16.0
K	0.1	13.4	26.8
	0.3	8.9	17.8
M	0.1	14.3	28.6
	0.3	10.3	20.7

- \mathcal{R}_1 : this region extends from 0.5 au to the snow line position at ~ 2.7 au (value for a primary G-type star). 200 particles were initially placed in this region.
- \mathcal{R}_2 : this region extends from beyond the snow line and up to the distance $a_{GG} - 3R_{H,GG} \approx 4.1$ au. We define this region as the inner disk. As we are mainly interested in icy bodies that are likely to bring water to the HZ, we densified this region and 1000 particles were distributed therein.
- \mathcal{R}_3 : this region extends from $a_{GG} + 3R_{H,GG} \approx 6.3$ au and up to the stability limit criteria defined by the critical semimajor axis a_c [Holman and Wiegert, 1999, Pilat-Lohinger and Dvorak, 2002] and its variance Δa_c . For the studied systems, the value of a_c are given in Tab. 1 using the method of Pilat-Lohinger and Dvorak [2002]. It is obvious that the size of the external disk will vary according to (a_b , e_b , M_b). The larger a_b and the smaller (e_b , M_b), the wider this region. We defined this region as the outer disk in which 1000 particles were placed.

For all three cases, the initial orbital separation between each particle is uniform and is defined as the ratio between the width of each region and the number of particles. Their initial motion is taken as nearly circular and planar. We also assumed all our asteroids in \mathcal{R}_2 and \mathcal{R}_3 with equal mass and an initial water mass fraction of 10%. Water mass loss due to ice sublimation was also taken into account during the numerical integrations. All the simulations are purely gravitational as we consider our numerical integrations to start as soon as the gas vanished (therefore we do not consider gas driven migration and eccentricity dampening). We also assumed that, at this stage, planetary embryos have been able to form. Our simulations were performed for 50 Myr using the Radau integrator in the Mercury6 package [Chambers, 1999].

3. Dynamics under the binary star perturbation

3.1. Orbit of the giant planet

Due to the secondary star, it is obvious that the gas giant will no longer remain on a circular motion. This is illustrated in Fig. 1 where the variation of the gas giant’s eccentricity e_{GG} is plotted for different values of the secondary’s periapsis distance q_b (35 au, 45 au, 70 au and 90 au) and for two different masses M_b (F- and M-type, on the top and bottom panel respectively). According to the secular theory, the variations of e_{GG} are linked to the oscillation period T of the giant planet and the amplitude depends on the mass and periapsis distance of the perturber. The higher M_b and the smaller q_b , the shorter T . In our case, T will

be shorter for the largest secondary's mass investigated (F-type) and smallest value of q_b (35 au). Therefore, we scaled the x-axis to this period¹ T_0 . For a given value of q_b , we can see that the secondary's mass does not have a major impact on the maximum value² of e_{GG} . For instance, for $q_b = 45$ au, we found that $e_{GG} \sim 0.04$ for any value of M_b . However, its period increases with q_b and M_b . Indeed, for $q_b = 35$ au, $T = T_0$ for a secondary F-type and $T = 4T_0$ if the secondary is a M-type star. Also, for $q_b = 90$ au, we have $T = 12T_0$ and $T = 40T_0$ for a secondary F- and M-type star, respectively. These periodic variations of e_{GG} will have consequences on the gravitational interaction with the disk of planetesimals.

The interaction with the disk will be strengthened as the gas

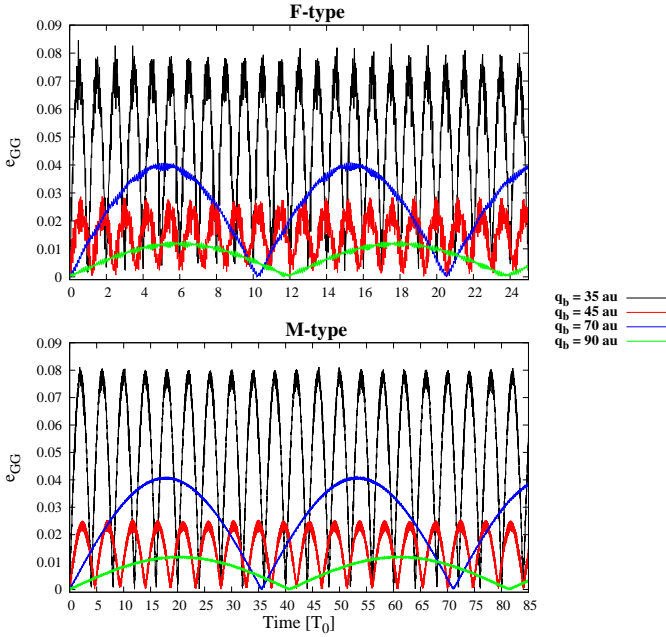


Fig. 1. Variation of the gas giant's eccentricity e_{GG} , under the perturbation of a secondary F-star (top) and M-star (bottom), as a function of time (expressed in T_0 units, see text) and for different secondary's periapsis distance q_b .

giant can encounter a semimajor axis drift. Indeed, we show in Fig. 2 that the dynamical perturbations induced by the secondary can slightly shift inward the initial semimajor axis of the gas giant by a quantity Δa_{GG} . Therefore, the location of MMRs will be affected as they mainly depend on a_{GG} . The consequences of such a drift will be analysed in section 3.3. region

3.2. Dynamics of the disk of planetesimals

We show in Fig. 3, the maximum eccentricity reached by the planetesimals at different initial semimajor axes, in the regions \mathcal{R}_1 and \mathcal{R}_2 (separated by the dashed vertical line representing the snow-line position). The four panels correspond to the values of q_b investigated and each subpanel is for different secondary

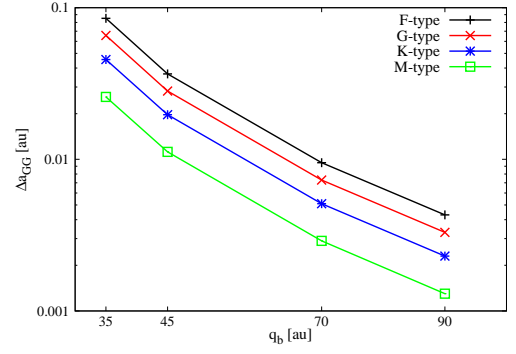


Fig. 2. Orbital inward shift Δa_{GG} of the gas giant as a function of the secondary's periapsis q_b and stellar type.

stellar types (F, G, K and M). We can distinguish MMRs³ with the gas giant and also a secular resonance: on the bottom panels representing the results for $a_b = 100$ au ($q_b = 70$ au and $q_b = 90$ au), we can see a spike located close to or inside the HZ⁴ (continuous vertical lines) and moving outward (to larger semi-major axes) when increasing the secondary's mass. This spike represents the secular resonance. When increasing q_b , not only it slightly moves inward but also, the maximum eccentricity reached by the particles is higher. This is because the gravitational perturbation from the secondary increases the gas giant's eccentricity. As a consequence, the forced eccentricity contribution of any particle inside the secular resonance will be increased. When decreasing a_b to 50 au (top panels for $q_b = 35$ au and $q_b = 45$ au), the secular resonance moves also outward and reaches the MMR region. As a consequence, the inner disk will suffer from an overlap of these orbital resonances that could cause a fast depletion. However, particles inside the HZ will remain on near circular motion. We should also notice, as studied in detail by Pilat-Lohinger et al. [2016], the combined effects induced by a change of e_b when the other dynamical parameters (a_b and M_b) remain constant. Indeed, an increase of e_b will turn into:

- an increase of e_{GG} (see Fig. 1) so that the size of the secular perturbed area is increased but the location remains the same;
- an inward shift of the gas giant with intensity depending on the binary star characteristics (see Fig. 2) where the width of the secular resonance remains unchanged but its location is shifted inward.

As a consequence, only the width (see top panels in Fig. 3) or both the location and the width of the secular resonance can be modified (see bottom panels in Fig. 3), as also shown in Pilat-Lohinger et al. [2016] and Bazsó et al. [2016].

The outer disk exhibits dynamical outcomes different from the inner disk. Indeed, only external MMRs⁵ and gravitational interactions with the gas giant perturb \mathcal{R}_3 . As pointed out in Fig. 1, in the case of $q_b = 35$ au, the periodic high variations of e_{GG} coupled with the gravitational excitation from the secondary, will cause a strong interaction with the external disk and its dynamical behaviour will be more or less chaotic. When increasing q_b (and therefore increasing the size of the disk and

³ Only the main ones are indicated

⁴ the borders are defined according to Kopparapu et al. [2013]

⁵ MMRs with the secondary star also influence the dynamics of celestial bodies and their location depends on the secondary star's orbital parameters. However, they have a very high order and their contribution is much weaker compared to the MMRs with the gas giant.

¹ The numerical value is $T_0 = 6323$ yr

² The difference does not exceed $\sim 0.5\%$

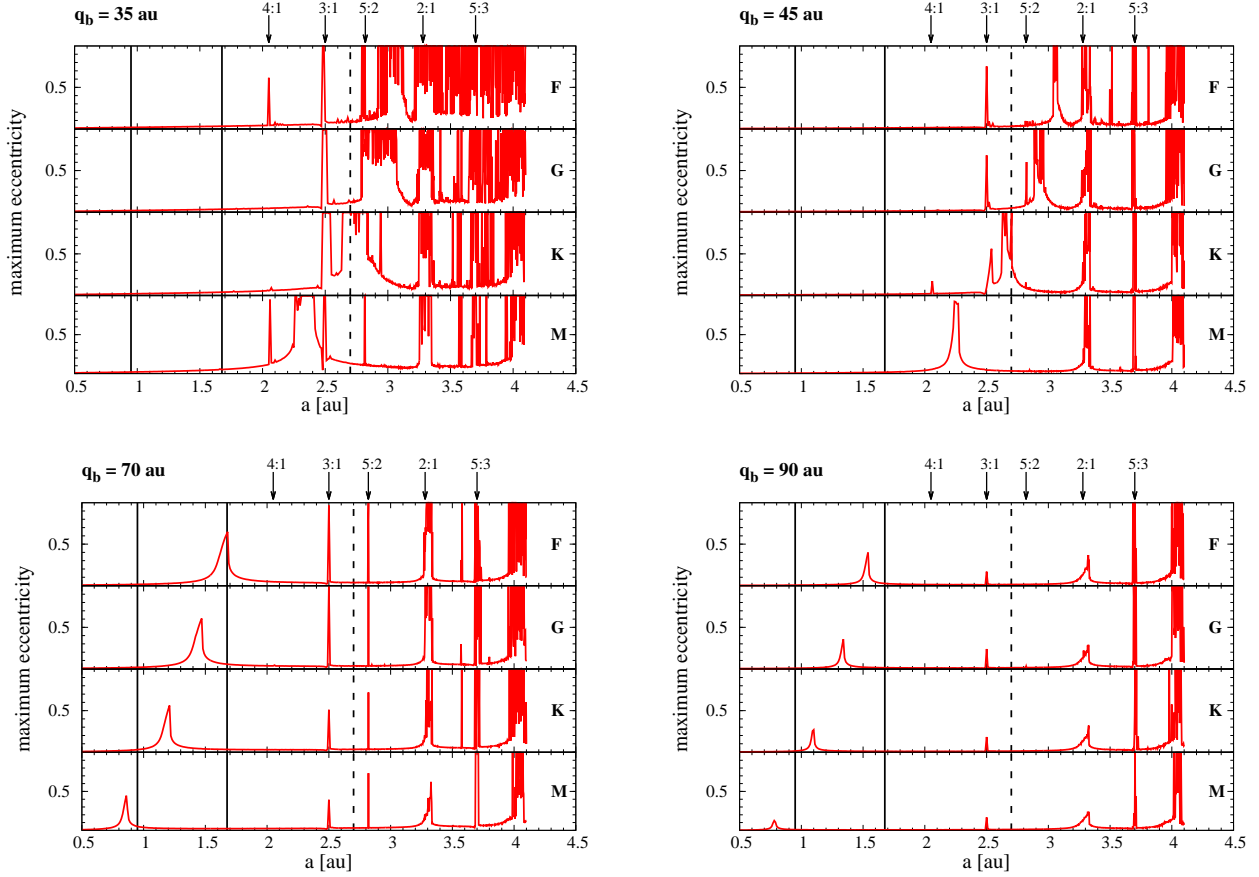


Fig. 3. Maximum eccentricity of planetesimals in the \mathcal{R}_1 and \mathcal{R}_2 regions, separated by the dashed vertical line for the snow line position, as a function of their initial position, up to an intermediate integration time of 5 Myr, for different values of q_b . Each subpanel refers to the secondary stellar type and the continuous vertical lines refer to the HZ borders. In addition, the inner main MMRs with the gas giant are indicated.

decreasing e_{GG}), the external MMRs dominate.

To highlight our results, we show in Fig. 4 the dynamical outcome of the \mathcal{R}_2 and \mathcal{R}_3 regions for a secondary F-type (left panel) and M-type (right panel) star. Because of the definition of \mathcal{R}_3 , a secondary F-type star at $q_b = 35$ au can not host an outer disk⁶. For this value of q_b , we can see that more than 80% of the inner disk escaped within 50 Myr. This is because the secular resonance lies inside \mathcal{R}_2 and its large width (see top right panel in Fig. 3 for the case of a secondary F-type) will favor chaos therein. Thus, this orbital resonance plays an important role for the depletion of a planetesimal disk. We expect similar results for a G- and K-type secondary as the secular resonance lies beyond the snow-line. This is not the case for an M-type at the same periastris distance and we can clearly see that the lack of strong perturbations inside \mathcal{R}_2 (the secular resonance is inside the snow-line, see top right panel in Fig. 3 for the case of a secondary M-type) enables 70% of the inner disk population to survive within 50 Myr. The evolution of the population in \mathcal{R}_3 will be strongly correlated to this region's width and to the gravitational interactions with the gas giant and the secondary star. The more compact is the outer disk and the stronger are the perturbations from the massive bodies, the more likely is the loss of asteroids in \mathcal{R}_3 .

This result can also question the presence and observational evidence of a remaining asteroid belt in such systems for $a_b = 50$ au, as an inner disk can suffer of both secular and mean motion perturbations but also of strong interactions with the gas giant. It might not survive under such conditions as we can observe a linear decrease of the population of \mathcal{R}_2 . Therefore, its dynamical lifetime will vary according to M_b .

3.3. Dynamical lifetime of particles near MMRs

In this section, we investigate in detail the dynamical lifetime of particles which are initially close or inside internal MMRs. They occur when the orbital periods of the gas giant and the particle are in commensurability such as:

$$a_n = \left(\frac{p}{q}\right)^{2/3} a_{GG}, \quad p \text{ and } q \in \mathbb{N} \begin{cases} p > q & \text{if } a_n < a_{GG} \\ p < q & \text{if } a_n > a_{GG} \end{cases}$$

where a_n is the position of the nominal resonance location. As shown in Fig. 2, the gas giant will have periodic variations in the interval $[a_{GG} - \Delta a_{GG}; a_{GG}]$. Thus, for a given pair (p,q), the maximum shift Δa_n of a_n is $(p/q)^{2/3} \Delta a_{GG}$. As we aim to correlate the dynamical lifetime of particles with the binary star characteristics, we preferred doing a separate analysis to ensure that each MMR contains the same number of particles. Indeed, our results would be biased if we use the sampling described in section 2.

⁶ as $a_c - \Delta a_c \leq a_{GG} + 3R_{H,GG}$

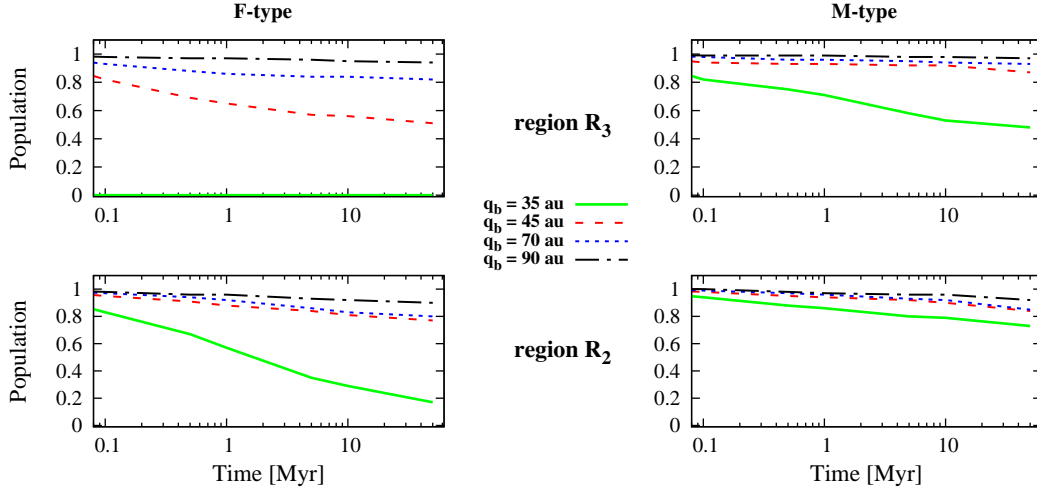


Fig. 4. Evolution of the remaining population in the \mathcal{R}_3 (top) and \mathcal{R}_2 (bottom) regions according to the periapsis distance q_b of a secondary F-type (left) and M-type (right) star.

Instead, for each MMR investigated, we defined an interval \mathcal{A}_n of initial semimajor axis for our test particles:

$$\mathcal{A}_n = [a_n - \Delta a_n - \epsilon; a_n + \epsilon'], \quad (\epsilon, \epsilon') \in \mathbb{R}$$

where (ϵ, ϵ') are arbitrary numbers⁷ in order to take into account particles initially orbiting near the MMR and likely to cross it during the integration. We limited this study to resonances with integers p and $q \leq 10$. In each MMR, we uniformly distributed 25 particles⁸ with a step-size depending on the size of \mathcal{A}_n , initially on circular and planar orbits. In addition, as suggested by Pilat-Lohinger and Dvorak [2002], each particle is cloned into four starting points with mean anomalies $M = 0^\circ$, $M = 90^\circ$, $M = 180^\circ$ and $M = 270^\circ$, as it is well known that the starting position plays an important role for the dynamical behaviour in MMRs. This accounts for 100 particles in each MMR. Each system was integrated for 50 Myr. We did not consider the condition $a \notin \mathcal{A}_n$ as a criterion for a particle to leave the MMR. Indeed, its dynamical evolution can be quite random: it can leave from time to time a MMR or be temporarily captured into another MMR. Instead, we consider a particle to leave its initial location in a specific MMR when its dynamical evolution leads to a collision with either one of the stars or the gas giant. Finally, we defined the dynamical lifetime of particles inside a specific MMR as the time required for 50% of the population to leave the resonance [Gladman et al., 1997]. We show in Fig. 5, the dynamical lifetime in Myr of particles near the internal MMRs. In the top panel of this figure, the influence of M_b is shown for a certain periapsis distance $q_b = 35$ au. The bottom panel summarizes the results for a certain mass of the secondary star (i.e. G-type star) and different periapsis distances of this star. For the top panel, we have chosen $q_b = 35$ au as for this particular value, the secular resonance overlaps with the MMRs in \mathcal{R}_2 . We can see that prior to the 8:3 MMR, the border between icy and rocky asteroids, a secondary M-type will favor chaos inside the rocky bodies region located in \mathcal{R}_1 . This is not surprising as Fig. 3 clearly shows the secular resonance overlapping with MMRs located inside the

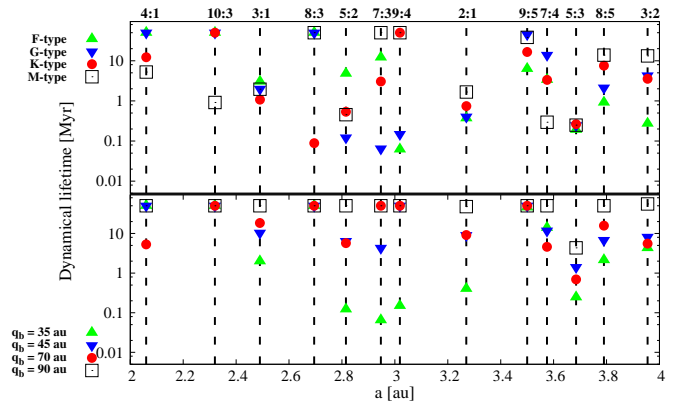


Fig. 5. Dynamical lifetime of test particles in \mathcal{R}_1 and \mathcal{R}_2 regions expressed in Myr. Top panel: influence of the secondary's mass when $q_b = 35$ au. Bottom panel: influence of the secondary's periapsis distance q_b assuming the secondary as a G-type star.

snow-line at 2.7 au. Beyond this limit, a higher value of M_b leads to a lower dynamical lifetime – values can reach 0.1 Myr – as the secular resonance will move outward. From the bottom panel, one can recognize that the lower q_b , the lower the dynamical lifetime. Some MMRs can be quickly emptied within 0.1 Myr. With these tests, we highlight that in binary star systems, the dynamical lifetime of particles initially orbiting inside or close to MMRs can be variable according to the location of the secular resonance. Provided that particles can reach the HZ region before colliding with one of the massive bodies (i.e. the stars or the gas giant) or before being ejected out of the system, they could rapidly cause an early bombardement on any embryos or planets moving in the HZ.

4. Asteroid flux and water transport to the HZ

In this section, we proceed in comparing the flux of icy particles from \mathcal{R}_2 and \mathcal{R}_3 towards the HZ. We recall the definition of Habitable Zone crossers (HZc) as defined in Paper I. HZc are any particles initially evolving beyond the snow line (2.7 au) and

⁷ $(\epsilon, \epsilon') \sim \pm 1\%$

⁸ We did not put more particles as \mathcal{A}_n is very narrow. In \mathcal{R}_2 , the size of \mathcal{A}_n is $\sim \Delta a_n \leq \Delta a_{GG}$ as $(p/q)^{2/3} \leq 1$. In \mathcal{R}_3 , we would have considered an other approach as the size of \mathcal{A}_n would be much wider because $(p/q)^{2/3} \geq 1$

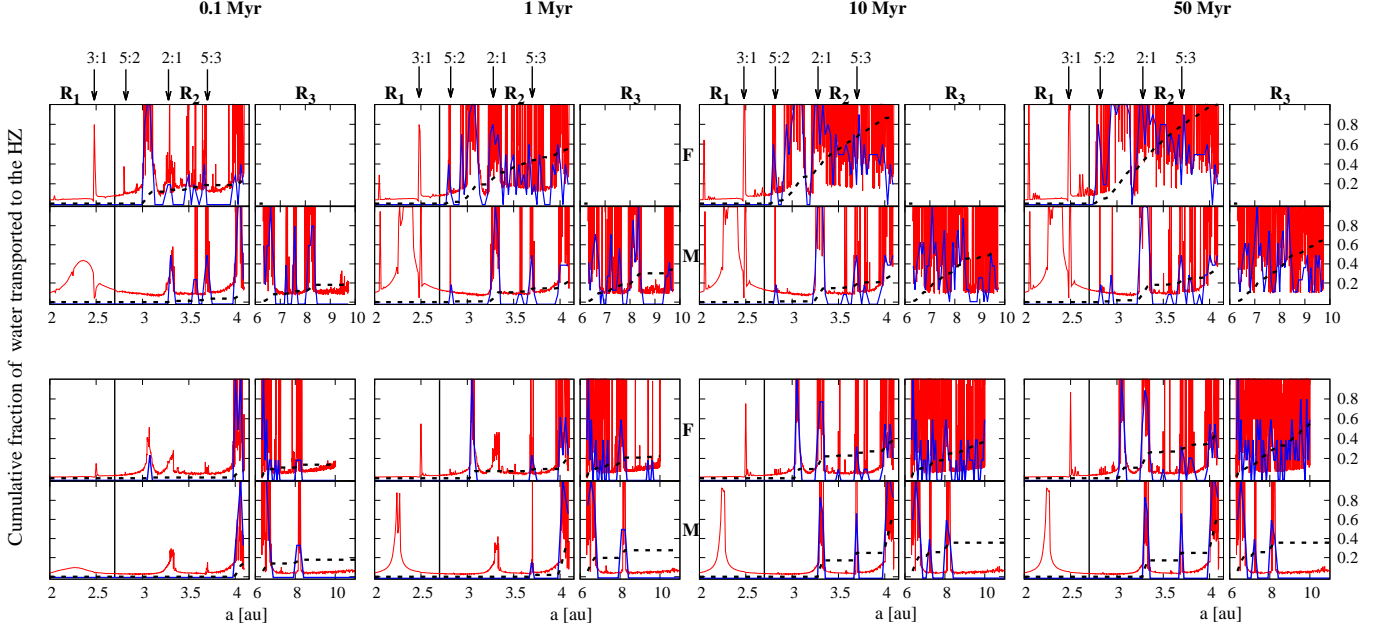


Fig. 6. We represented on the y-axis (left and right axes have the same scale), the variation of the maximum eccentricity (red line) together with the cumulative fraction of water (dashed black line) brought to the HZ, with respect to the initial location of small bodies in \mathcal{R}_2 and \mathcal{R}_3 . The top panel is for a secondary star at $q_b = 35$ au and the bottom panel is for $q_b = 45$ au. For each panel, two examples are shown for a secondary F-type (top subpanel) and M-type (bottom subpanel) star. The cumulative fraction of water is determined with respect to the final amount of water transported from \mathcal{R}_2 and \mathcal{R}_3 , within 50 Myr. We also represented on this figure, the normalized HZc distribution (blue line) calculated according to the total number of HZc produced for each period of integration time from 0.1 Myr (left) up to 50 Myr (right). The vertical black line refers to the position of the snow line. The entire region \mathcal{R}_3 is intentionally not displayed because of its size. Instead, only the dynamically interesting part of \mathcal{R}_3 is shown.

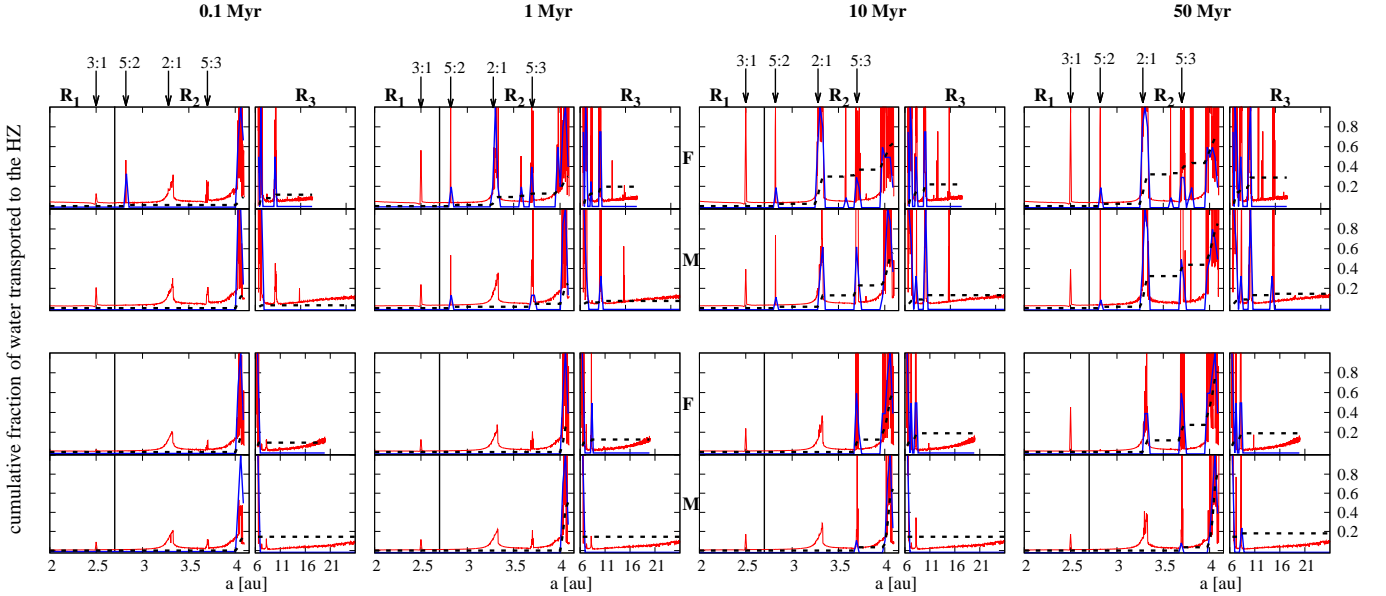


Fig. 7. Same as for Fig. 6 but for $q_b = 70$ au (top panel) and $q_b = 90$ au (bottom panel).

crossing at least once the HZ within the integration time. These authors showed that the higher M_b and q_b , the more important the rate of HZc and therefore the quantity of water transported to the HZ. We analyse here how the orbital resonances influence the asteroid flux to the HZ and the amount of water beared therein. We represent on the y-axis in Fig. 6, the evolution of the

maximum eccentricity (red line) of particles inside \mathcal{R}_1 , \mathcal{R}_2 (as already drawn in Fig. 3) and \mathcal{R}_3 . The top panel corresponds to a secondary star at $q_b = 35$ au and the bottom panel is for $q_b = 45$ au, each subpanel corresponding either to a secondary F- or M-type star. We chose these two cases to highlight the impact of the location of the secular resonance when it lies inside the snow-

line (M-type) and beyond the snow-line (F-type). From left to right, each figure is for a different period of integration (between 0.1 Myr to 50 Myr). We also show the normalized HZc distribution (blue line) calculated regarding the total number of HZc produced by the corresponding systems for each period of integration time. For all considered cases, within 10 Myr, the 2:1 MMR located at ~ 3.28 au and the secular resonance, when it lies beyond the snow-line, are the primary sources of HZc in the inner disk. In addition, the external disk can produce a non negligible or equivalent number of HZc, compared to the inner disk. Indeed, as mentioned in section 2, the smaller is q_b the more compact is the outer disk. In this case, the depletion can be fast and the dynamics is more chaotic. As a result, asteroids might not cross the HZ before colliding with the stars and the gas giant or being ejected. In order to estimate the amount of transported water, we followed the same approach as in Paper I i.e. the contribution of the maximum water content of all the HZc when they first cross the HZ. On the same figure, the y-axis corresponds also to the cumulative fraction of water (dashed black line) brought by the HZc. This fraction is determined with respect to the final number of transported water from \mathcal{R}_2 and \mathcal{R}_3 within 50 Myr. As already mentioned in section 2, a system with a F-star as a companion and $q_b = 35$ au can not host an outer disk. Therefore, all the incoming water in the HZ, for this particular system, is from \mathcal{R}_2 . All our systems exhibit the same trend: the quantity of incoming water inside the HZ drastically increases when particles orbit initially inside the secular resonance and the 2:1 MMR. We show similar results in Fig. 7 for $q_b = 70$ au (top panel) and $q_b = 90$ au (bottom panel). Contrary to the previous case, the secular resonance does not contribute at all in bearing water material into the HZ as it lies in this region (see Fig. 3). We show that the two main sources of HZc in \mathcal{R}_2 are the 2:1 and 5:3 MMR. The contribution of \mathcal{R}_3 is more negligible than in the previous case as its size is more extended and weakly perturbed.

5. Influence of the dynamical parameters on the planetesimal disk

We are now interested in how the previous results, mainly the origin of HZc and the water transport to the HZ, are influenced by the gas giant's dynamical and physical parameters or when considering the case of one or two gas giants orbiting a single star. The same number of particles were placed in the three regions⁹ as defined in section 2 but we did not repeat the simulations for all the binary systems investigated in the previous sections. Instead, we selected two for comparison: a secondary F-type with $q_b = 45$ au and a secondary M-type with $q_b = 70$ au. Thus, comparison of the results from this section and illustrated in Fig. 8 will be made with the bottom panels in Fig. 6 (top figure for the F-type) and top panels in Fig. 7 (bottom figure for the M-type). The results shown in Fig. 8 correspond only to 10 Myr of integration time.

5.1. The gas giant's orbital and physical parameters

We investigated different cases in order to separately highlight the influence of the initial parameters a_{GG} , e_{GG} and M_{GG} . The results are shown on the left panels in Fig. 8:

- case 1 (top panel): we increase the initial eccentricity to $e_{GG} = 0.2$. For both cases (F- and M-types), the participation of \mathcal{R}_2 in the water transport to the HZ is much more important

than \mathcal{R}_3 , as region \mathcal{R}_2 is mainly dominated by chaos. Indeed, in addition to stronger interactions with the disk, the width of the secular resonance will be increased, for the case of the secondary F-type star, as pointed out in Pilat-Lohinger et al. [2016]. Both strong mechanisms explain the higher flux of asteroids towards the HZ in comparison with $e_{GG} = 0.0$.

- case 2 (middle panel): we change the initial gas giant's semi-major axis to $a_{GG} = 4.5$ au and 6.0 au. As a consequence, the secular resonance will be shifted inward or outward respectively. For a secondary F-type for instance, the semi-analytical method developed by Pilat-Lohinger et al. [2016] predicts an inward shift close to the 5:2 MMR (inside the snow-line) or an outward shift beyond the 2:1 MMR, respectively. Furthermore, for both cases (F- and M-types), decreasing a_{GG} to 4.5 au will result in shifting the 5:2 MMR inside \mathcal{R}_1 (therefore it will not participate in bearing water to the HZ) whereas increasing a_{GG} to 6.0 au will result in shifting the 3:1 MMR inside \mathcal{R}_2 (thus it will participate in moving icy asteroids from beyond the snow-line to the HZ region).
- case 3 (bottom panel): we change the mass of the gas giant to $M_{GG} = 3M_J$ and $M_J/3$. For the case of a secondary F-type star for instance, the theoretical location of the secular resonance will be shifted inward for $M_{GG} = 3M_J$ (the secular resonance is below the 3:1 MMR) and outward for $M_{GG} = M_J/3$. For both secondaries (F- and M-types), the MMRs produce a significant amount of HZc within 0.1 Myr for $M_{GG} = 3M_J$ and 10 Myr for $M_{GG} = M_J/3$ whereas 1 Myr is needed for $M_{GG} = 1M_J$.

5.2. The case of single star systems

In case only one star is present in the system, we aim to compare the previous results with the case of one or two giant planets orbiting a G2V star. We study three possibilities for the giant planets' configurations and the corresponding results are shown on the right panels in Fig. 8:

- case 1 (top panel): one Jupiter at 5.2 au initially on a circular orbit
- case 2 (middle panel): one Jupiter at 5.2 au initially on an elliptic orbit with $e_{GG} = 0.2$
- case 3 (bottom panel): a system with two giant planets i.e. a Jupiter and a Saturn¹⁰

For the three cases, the value of the outer border of \mathcal{R}_3 is equal to the highest value of a_c in Tab. 1 (i.e. a wide outer disk). The value of the inner border of \mathcal{R}_3 is calculated taking into account the Hill radius of the outer giant planet (i.e. the Jupiter-like for one gas giant and the Saturn-like if the system contains two gas giants). Unsurprisingly, because of the lack of strong perturbations¹¹, only small bodies initially orbiting close to the gas giant can become HZc in case 1. The flux of icy asteroids drastically increases as soon as the initial eccentricity of the gas giant is increased (case 2): the interaction with the disk is stronger and it is not obvious to identify the most efficient MMR in producing HZc but the region \mathcal{R}_2 is the main source of water. In contrast, the contribution of \mathcal{R}_3 in the case 3 is as important as for \mathcal{R}_2 because of the presence of the second gas giant. Contrary to the

⁹ The size of \mathcal{R}_2 and \mathcal{R}_3 can vary because of R_{HGG}

¹⁰ their mass and initial orbital elements are the commonly used ones

¹¹ there cannot be a secular resonance; only MMRs can perturb the asteroids' orbits

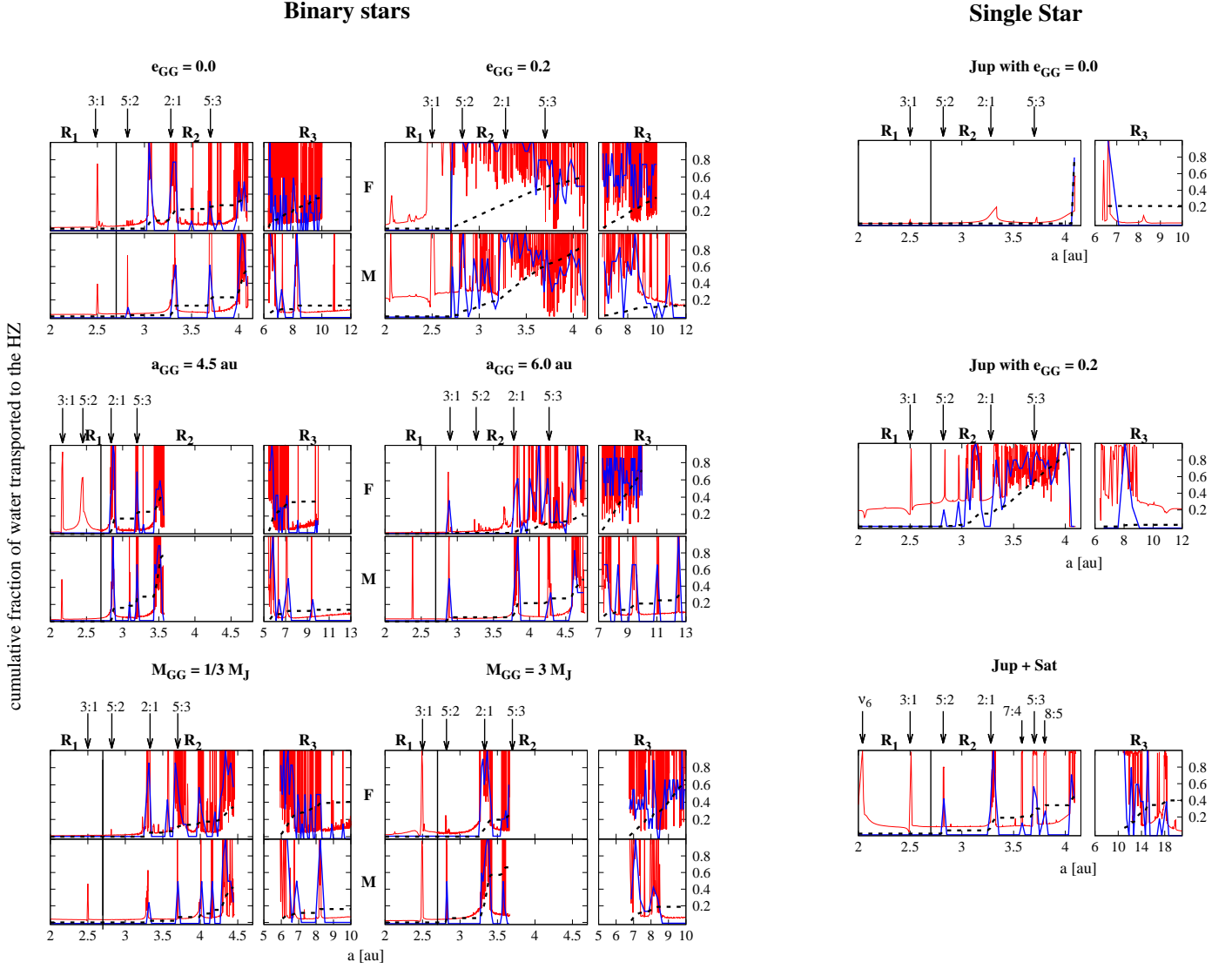


Fig. 8. Left: influence of the gas giant’s orbital and physical parameters. Top and bottom subpanels are for a secondary F-type and M-type star, respectively. Right: the three subpanels show results for the case of single star systems. Each plots correspond to an intermediate integration time of 10 Myr. See text in section 5 and legend of Fig. 6 for more details.

binary cases in which the 2:1 MMR and the secular resonance (when lying inside \mathcal{R}_2 , see Fig. 6) were the primary sources of HZc within the whole integration time, in case 3, the 2:1 MMR becomes dominant only within 10 Myr of integration. Below 10 Myr, the 5:2 and 5:3 MMRs dominate over the other MMRs.

6. Comparison of the water transport efficiency

Finally, we combine in Fig. 9 the results obtained in sections 4 and 5 in order to compare the total fraction of water transported into the HZ, expressed with respect to the initial total amount of water in the disk. The top panel compiles the results obtained in section 4 for a secondary F-type (left) and M-type (right). The middle panel compiles the results from section 5.1 when changing the gas giant’s orbital and physical parameters, for a secondary F-type at $q_b = 45$ au and a secondary M-type at $q_b = 70$ au. Finally, the bottom panel shows the results for single star systems containing one or two gas giants.

In the binary cases, when the parameters of the gas giant are

fixed (top panels), one can see for instance, that a secondary M-type star at $q_b = 35$ au, needs ~ 50 Myr so that one quarter of the water initially in the disk of planetesimals is transported to the HZ, contrary to an F-type star where only ~ 0.5 Myr is needed. This is mainly due to the presence of the secular resonance inside the asteroid belt in \mathcal{R}_2 .

When changing the gas giant’s orbital and physical parameters (middle panels), the water transport efficiency to the HZ can be different (comparisons have to be made with the red-dashed line for the secondary F-star at $q_b = 45$ au and the blue-dotted line for the M-type at $q_b = 70$ au in the top panels). For instance, the figure reveals that increasing e_{GG} boosts the water transport efficiency. Indeed, within 0.1 Myr, almost 50% of the initial water ended in the HZ for the case of a F-star, and nearly 20% for an M-type¹². When changing a_{GG} , even with the lack of active orbital resonances for the case of $a_{GG} = 4.5$ au (the 5:2 MMR and the secular resonance lie inside the snow-line), the 2:1 and

¹² For both cases, this is 2.5 times more than for the case $e_{GG} = 0$

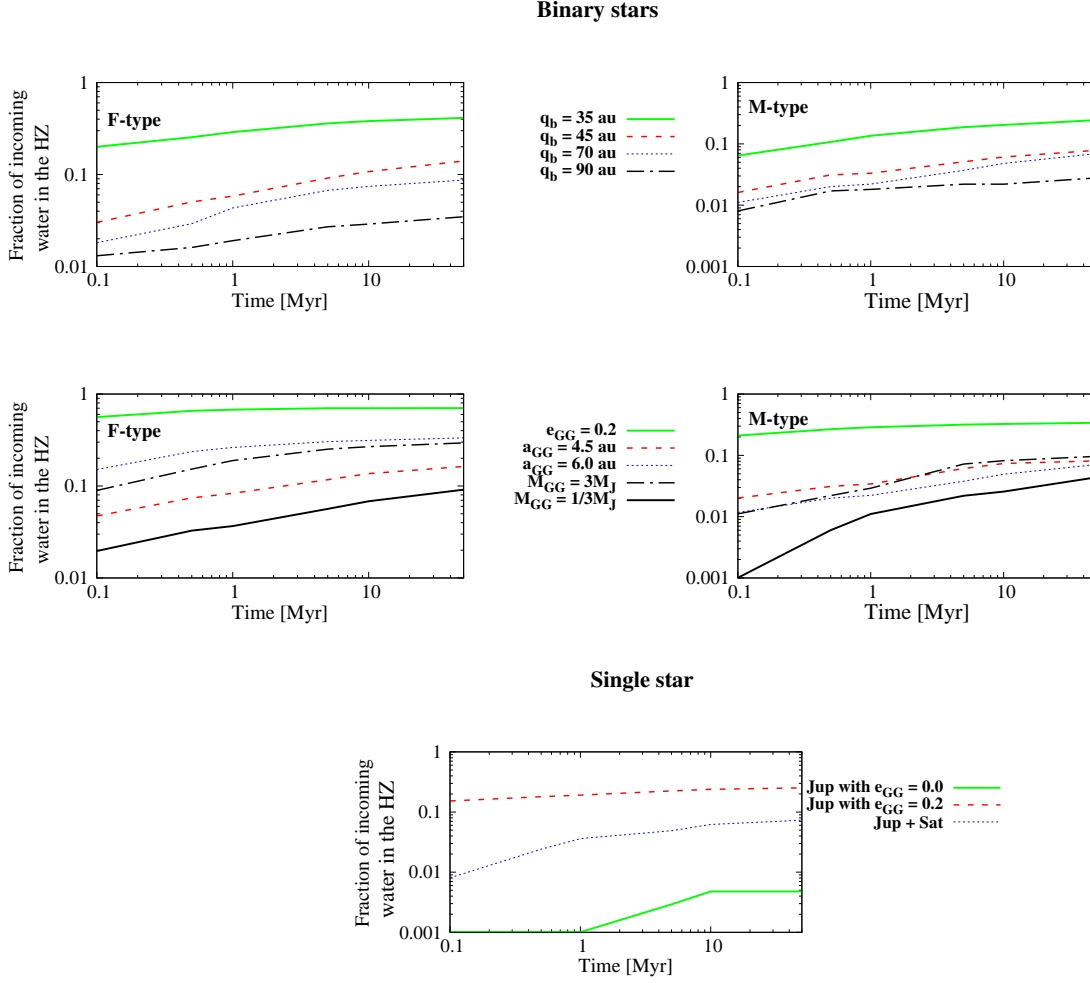


Fig. 9. Fraction of incoming water in the HZ with respect to the initial total amount of water in the disk of planetesimals, considering various configurations: Top and middle panels show results in binary star systems for fixed and variable values of the gas giant’s orbital and physical parameters respectively, when the secondary is an F-type (left) and M-type (right) star (see text in section 5.1). Comparison with various single star systems are shown in the bottom panel (see text in section 5.2).

5:3 MMR are powerful enough so that the water transport is as efficient as for a giant planet at $a_{GG} = 5.2$ au. For $a_{GG} = 6.0$ au, as the 3:1 MMR participates in the asteroid flux, the water transport is even more efficient. The mass of the gas giant also influences the final total amount of water brought to the HZ as a higher or smaller value of M_{GG} will respectively strengthen or weaken the water transport efficiency of a binary star system.

Finally, comparable results (bottom panel) can be obtained with different single star configurations hosting either one or two giants planets. If only one giant planet, with $e_{GG} = 0.0$, orbits a sun-like star, a significant water transport in the HZ within 50 Myr is very unlikely because of the lack of gravitational perturbations. However, if the gas giant initially starts on an eccentric orbit ($e_{GG} = 0.2$), the depletion of \mathcal{R}_2 will be quite fast and within 0.1 Myr, the water transport efficiency can be comparable to a secondary F-type star at $q_{GG} = 45$ au within 50 Myr. This is not surprising as such high eccentricity will favor chaos in \mathcal{R}_2 . Last but not least, if two giant planets (Jupiter and Saturn-like) orbit a sun-like star, both regions \mathcal{R}_2 and \mathcal{R}_3 are water sources as several inner and outer MMRs with the giant planets are active and 50 Myr are needed to transport 10% of the water initially present in

the disk. These results are comparable to the binary star systems simulations with an M-type as a companion.

7. Conclusion

We showed that the flux of icy bodies towards circumprimary HZs in binary star systems can vary according to the characteristics and motion of the secondary star and the giant planet. First, we showed that a gas giant planet can suffer from both variations of its orbital eccentricity and a drift in semi-major axis. This in turn would strengthen the interaction with an inner (region \mathcal{R}_2) and outer (region \mathcal{R}_3) disk of planetesimals. Moreover we highlight that in tight binaries ($a_b = 50$ au), a secular resonance can lie within the inner asteroid belt, overlapping with MMRs, which enable, in a short timescale, an efficient and significant flux of icy asteroids towards the HZ, in which particles orbit in a near circular motion (region \mathcal{R}_1). In contrast thereto, in the study of wide binaries ($a_b = 100$ au), particles inside the HZ can move on eccentric orbits when the secular resonance lies in the HZ. The outer asteroid belt is only perturbed by MMRs. As a consequence, a longer time is needed to produce a significant flux of icy asteroids towards the HZ. Such dynamics will

drastically impact the dynamical lifetime of particles initially located inside inner MMRs. Indeed, it can range from thousands of years to several million years according to the location of the MMR within the secular resonance. This can favor a fast and significant contribution of MMRs in producing HZ crossers (called HZc which are asteroids with orbits crossing the HZ) and bearing water therein. In any cases, we highlighted that, for the studied binary star systems, the inner disk (region \mathcal{R}_2) is the primary source of HZc (and therefore water in the HZ), by the means of the 2:1 MMR, the 5:3 MMR and the secular resonance, when this latter lies close or beyond the snow-line. As shown in section 5.1, the gas giant's characteristics also influence the asteroids flux to the HZ and therefore the water transport. Indeed, the dynamical interactions can be different as the location of the orbital resonances can be shifted inward or outward. Giant planets initially on eccentric orbits are an efficient way to ensure that the HZ can be rapidly fed with water (within 0.1 Myr) as it can increase the width of the secular resonance for instance. Even gas giants with lower mass can be efficient in the water transport to the HZ but on a longer timescale. For any giant planet configuration studied, the 2:1 MMR and 5:3 MMR also appeared to be powerful perturbations to transport water into the HZ. This is not necessarily the case in single star systems. In Jupiter and Saturn-like systems orbiting a sun-like star, other inner and outer MMRs are also, to a less extent, water sources.

As for the amount of transported water that effectively ends up on embryos and planets in the HZ, both Fig. 3 and Paper I have pointed out two opposite behaviours depending on the binary's orbit: a high rate of HZc and nearly circular motion in the HZ (tight binary) versus low rate of HZc and eccentric orbits in the HZ (wide binary). The main problems of the tight-binary case are:

- planets or embryos moving on nearly circular motion in the HZ will have lower impact probabilities with HZc – regarding also the water distribution within the HZ as shown in Paper I – than if they were moving on eccentric orbits;
- the asteroid flux to the HZ is a fast process. In case the primary star is in the T-Tauri phase, Tu et al. [2015] showed that the activity of a present Sun-like star can have a different history because of its rotational behaviour. As a consequence, planetary embryos might not be able to keep the incoming water at their surface;
- considering this last point and that the depletion of the inner disk (region \mathcal{R}_2) can be quite fast, there would not be other water sources available after the activity of the primary star has significantly decreased, if the remaining asteroids (in the inner and outer disk) stay on stable orbits.

In wide binaries, as the flux process is much slower, the activity of a young primary star would not be an obstacle for a planet to keep the water beared from asteroids at its surface, even if it loses its primary surface water content. Indeed, the eccentric motion inside the HZ can be a positive aspect: as planetary embryos can leave the HZ from time to time, they can increase their impact probabilities as they can also interact with icy asteroids evolving beyond the outer border of the HZ. However, the high eccentric motion inside the HZ can also raise some problems that would be subject of future studies.

Acknowledgements. DB and EPL acknowledge the support of the Austrian Science Foundation (FWF) NFN project: "Pathways to Habitability", subproject S11608-N16 "Binary Star Systems and Habitability". DB and EPL acknowledge also the Vienna Scientific Cluster (VSC project 70320) for computational

resources. AB and EPL acknowledges the support of the FWF project P22603-N16.

References

- D. Bancelin, E. Pilat-Lohinger, S. Eggli, T. I. Maindl, C. Schäfer, R. Speith, and R. Dvorak. Asteroid flux towards circumprimary habitable zones in binary star systems. I. Statistical overview. *A&A*, 581:A46, September 2015.
- Á. Bazsó, E. Pilat-Lohinger, S. Eggli, B. Funk, and D. Bancelin. A survey of secular resonances in circumstellar planetary systems of known binary stars. *in prep.*, 2016.
- C. Briceño, A. K. Vivas, N. Calvet, L. Hartmann, R. Pacheco, D. Herrera, L. Romero, P. Berlind, G. Sánchez, J. A. Snyder, and P. Andrews. The CIDA-QUEST Large-Scale Survey of Orion OB1: Evidence for Rapid Disk Dissipation in a Dispersed Stellar Population. *Science*, 291:93–97, January 2001.
- J. E. Chambers. A hybrid symplectic integrator that permits close encounters between massive bodies. *MNRAS*, 304:793–799, April 1999.
- B. J. Gladman, F. Migliorini, A. Morbidelli, V. Zappala, P. Michel, A. Cellino, C. Froeschle, H. F. Levison, M. Bailey, and M. Duncan. Dynamical lifetimes of objects injected into asteroid belt resonances. *Science*, 277:197–201, 1997.
- R. Gomes, H. F. Levison, K. Tsiganis, and A. Morbidelli. Origin of the cataclysmic Late Heavy Bombardment period of the terrestrial planets. *Nature*, 435:466–469, May 2005.
- N. Haghighipour and S. N. Raymond. Habitable Planet Formation in Binary Planetary Systems. *ApJ*, 666:436–446, September 2007.
- M. J. Holman and P. A. Wiegert. Long-Term Stability of Planets in Binary Systems. *AJ*, 117:621–628, January 1999.
- R. K. Kopparapu, R. Ramirez, J. F. Kasting, V. Eymet, T. D. Robinson, S. Mahadevan, R. C. Terrien, S. Domagal-Goldman, V. Meadows, and R. Deshpande. Habitable Zones around Main-sequence Stars: New Estimates. *ApJ*, 765:131, March 2013.
- A. Morbidelli, J. Chambers, J. I. Lunine, J. M. Petit, F. Robert, G. B. Valsecchi, and K. E. Cyr. Source regions and time scales for the delivery of water to Earth. *Meteoritics and Planetary Science*, 35:1309–1320, November 2000.
- L. R. Mudryk and Y. Wu. Resonance Overlap Is Responsible for Ejecting Planets in Binary Systems. *ApJ*, 639:423–431, March 2006.
- C. D. Murray and S. F. Dermott. *Solar system dynamics*. 1999.
- D. P. O'Brien, K. J. Walsh, A. Morbidelli, S. N. Raymond, and A. M. Mandell. Water delivery and giant impacts in the 'Grand Tack' scenario. *Icarus*, 239: 74–84, September 2014.
- E. Pilat-Lohinger. Planetary motion in double stars: the influence of the secondary. In Z. Knežević and A. Milani, editors, *IAU Colloq. 197: Dynamics of Populations of Planetary Systems*, pages 71–76, February 2005.
- E. Pilat-Lohinger and R. Dvorak. Stability of S-type Orbits in Binaries. *Celestial Mechanics and Dynamical Astronomy*, 82:143–153, February 2002.
- E. Pilat-Lohinger, Á. Süli, P. Robutel, and F. Freistetter. The Influence of Giant Planets Near a Mean Motion Resonance on Earth-like Planets in the Habitable Zone of Sun-like Stars. *ApJ*, 681:1639–1645, July 2008.
- E. Pilat-Lohinger, Á. Bazsó, and B. Funk. Circumstellar Multi-planetary systems in binary stars: secular resonances and a semi-analytical approach to determine its location. *in prep.*, 2016.
- G. Rabl and R. Dvorak. Satellite-type planetary orbits in double stars - A numerical approach. *A&A*, 191:385–391, February 1988.
- P. Thebault and N. Haghighipour. Planet formation in Binaries. *ArXiv e-prints*, June 2014.
- K. Tsiganis, R. Gomes, A. Morbidelli, and H. F. Levison. Origin of the orbital architecture of the giant planets of the Solar System. *Nature*, 435:459–461, May 2005.
- L. Tu, C. P. Johnstone, M. Güdel, and H. Lammer. The extreme ultraviolet and X-ray Sun in Time: High-energy evolutionary tracks of a solar-like star. *A&A*, 577:L3, May 2015.
- K. J. Walsh, A. Morbidelli, S. N. Raymond, D. P. O'Brien, and A. M. Mandell. A low mass for Mars from Jupiter's early gas-driven migration. *Nature*, 475: 206–209, July 2011.